Helical epitope of the group B meningococcal α(2–8)-linked sialic acid polysaccharide

ARTICLE *in* BIOCHEMISTRY · JULY 1992

Impact Factor: 3.02 · DOI: 10.1021/bi00136a012 · Source: PubMed

Helical Epitope of the Group B Meningococcal α(2-8)-Linked Sialic Acid Polysaccharide†

Jean-Robert Brisson,‡ Herbert Baumann,‡ Anne Imberty,§ Serge Pérez,§ and Harold J. Jennings*,‡

Institute for Biological Sciences, National Research Council of Canada, Ottawa, Canada K1A OR6, and Laboratoire de Physicochimie des Macromolécules, Institut National de la Recherche Agronomique, BP 527, 44026 Nantes Cédex, France

Received December 28, 1991; Revised Manuscript Received March 11, 1992

ABSTRACT: The immunological properties of the group B meningococcal α(2-8)-linked sialic acid polysaccharide have been rationalized in terms of a model where the random coil nature of the polymer can be described by the presence of local helices. The conformational versatility of the αNeuAc(2-8)αNeuAc linkage has been explored by NMR studies at 600 MHz in conjunction with potential energy calculations for colominic acid, an α(2-8)NeuAc polymer, and the trisaccharide αNeuAc(2-8)αNeuAc(2-8)βNeuAc. Potential energy calculations were used to estimate the energetically favorable conformers and to describe the wide range of helices which the polymer can adopt. No unique conformer was found to satisfy all NMR constraints, and only ensemble averaged nuclear Overhauser enhancements could correctly simulate the experimental data. Conformational differences between the polymer and the trisaccharide could be best explained in terms of slight changes in the relative distribution of conformers in solution. Similar helical parameters for the α(2-8)NeuAc polymer and poly(A) were proposed as the basis for their cross-reactivity to a monoclonal antibody IgM^{NOV}. The unusual length dependency for binding of oligosaccharide to group B specific antibodies was postulated to arise from the recognition of a high-order local helix with an extended conformation which was not highly populated in solution.

Group B *Neisseria meningitidis* and *Escherichia coli* K1 are major causes of meningitis. Both bacteria have identical capsular polysaccharides composed of α(2-8)-linked sialic acid residues. Although vaccine development has been hampered by the poor immunogenicity of the group B meningococcal polysaccharide in humans, by N-propionylation of its sialic acid residues, antibodies are produced which are both bactericidal and protective [for reviews, see Jennings (1989, 1990)].

The α(2-8)-linked sialic acid homopolymer has many interesting immunological properties which have been extensively studied. The presence of a conformational epitope was hypothesized by Jennings et al. (1984) to explain the inability of oligosaccharides of up to five residues to inhibit the binding of the group B polysaccharide to a homologous horse antibody. Later, it was established that an unusually large decasaccharide was required to bind or inhibit group B polysaccharide specific antibodies (Jennings et al., 1985; Finne & Makela, 1985; Hayrinen et al., 1989). This is in contrast with a conventional sequential oligomer where only a maximum 6 or 7 residues are necessary for binding (Kabat, 1960). Cross-reactivity of a human monoclonal antibody (IgM^{NOV}) with the α(2-8)NeuAc[1] polymer, poly(A), and other polynucleotides has also been observed (Kabat et al., 1988).

Various attempts have been made to relate these immunological properties to the three-dimensional structure of the antigen. Lindon et al. (1984), from NMR studies at 360 MHz, determined differences in the orientation of the exocyclic chains of the α(2-8)NeuAc and α(2-9)NeuAc polysaccharides and in the segmental motion of the polysaccharides. Michon et al. (1987) determined from NMR studies at 500 MHz that the conformation of the linkages of the polysaccharide and short oligosaccharides were different. Yamasaki and Bacon (1991), from a quantitative analysis of 2D NOE's at 500 MHz using rigid models, suggested that the polysaccharide adopts ordered helical structures in solution. In the present paper, the conformational properties of colominic acid, an α(2-8)-NeuAc polymer, and the trisaccharide αNeuAc(2-8)-αNeuAc(2-8)βNeuAc were evaluated by NMR studies at 600 MHz, in conjunction with potential energy calculations. The interpretation of the NOE's was based on a model which allows for the inherent flexibility about the linkages. The conformational versatility of the molecule was estimated by potential energy calculations. The biological implications were rationalized in terms of a model where the random coil nature of a polysaccharide can be described by the presence of local helices (Perez & Vergelati, 1985).

Experimental Procedures

Nuclear Magnetic Resonance Experiments. The colominic acid polysaccharide and the trisaccharide were prepared as described before (Michon et al., 1987), at concentrations of 10–20 mg in 0.5 mL of 95% D_2O, 5% acetone-d_6, pH 7, Na^+ counterion. Samples were purged with helium gas. Upon storage at a cold temperature, samples in solution were found to be stable for months, with no signs of degradation. The H3a and H3e resonances of the reducing terminus were partially deuterated (>50%) after several months in solution. All experiments were performed on a Bruker AMX 600 spectrometer at 288 K. For additional temperature stability, the deuterium lock was established on internal acetone-d_6. No significant changes in chemical shift were observed upon the addition of acetone-d_6. For colominic acid, pure absorption phase sensitive 2D NOE experiments were done in TPPI mode (Bodenhausen et al., 1984) with six mixing times of 25, 50, 75, 100, 150, and 200 ms. The relaxation delay between

† This is National Research Council of Canada Publication No. 32011. Part of this work was made possible through the France–Canada exchange program granted to J.R.B. and financial support from INRA.

‡ National Research Council of Canada.

§ Institut National de la Recherche Agronomique.

[1] Abbreviations: COSY, correlation spectroscopy; NeuAc, *N*-acetylneuraminic acid; NOE, nuclear Overhauser enhancement; NMR, nuclear magnetic resonance; TPPI, time-proportional phase increments.

0006-2960/92/0431-4996$03.00/0 Published 1992 by the American Chemical Society

Table I: MM2-Minimized Coordinates of αNeuAc–O–Me

atom	X	Y	Z
C1	2.00350	−0.00013	1.42684
C2	1.42467	0.00407	0.00253
C3	1.85264	1.28886	−0.71271
C4	3.33580	1.26891	−1.05815
C5	3.63666	0.02645	−1.89345
C6	3.16028	−1.22252	−1.14587
C7	3.36974	−2.51478	−1.94809
C8	2.79059	−3.75974	−1.27483
C9	3.14742	−5.05286	−1.99458
C10	5.59251	−0.31857	−3.37196
C11	7.10639	−0.36067	−3.44988
O1a	1.35286	0.85734	2.23587
O1b	2.93208	−0.64255	1.83271
O2	0.01649	−0.00037	0.00817
O4	3.67387	2.43642	−1.80927
O6	1.78881	−1.12261	−0.78919
O7	2.77959	−2.38247	−3.24501
O8	3.28173	−3.86537	0.06502
O9	2.61127	−6.11483	−1.24381
O10	4.90479	−0.55473	−4.34865
N5	5.06865	−0.02067	−2.13024
H3a	1.26995	1.39780	−1.65856
H3e	1.61658	2.18718	−0.09476
H4	3.95711	1.27566	−0.13132
H5	3.07491	0.12311	−2.85219
H6	3.76751	−1.31926	−0.21869
H7	4.46117	−2.67404	−2.11132
H8	1.67985	−3.67829	−1.20742
H9R	4.25246	−5.18468	−2.05049
H9S	2.71761	−5.10088	−3.02114
H11a	7.50134	−1.14014	−2.75920
H11b	7.53118	0.62782	−3.16186
H11c	7.44975	−0.60184	−4.48183
HN5	5.72929	0.09162	−1.36044
HO1a	1.79198	0.79277	3.09998
HO4	4.54535	2.33014	−2.15201
HO7	3.35196	−1.87683	−3.79615
HO8	4.20238	−3.66611	0.05735
HO9	2.75650	−5.93429	−0.33581
CM2	−0.56945	−1.16138	0.57428
HM2a	−0.19855	−1.33684	1.60824
HM2b	−0.37743	−2.05165	−0.06578
HM2c	−1.66970	−0.99793	0.61710

acquisitions was 6 s, and the sweep width was 2400 Hz. Matrices of 512 by 2048 points were recorded with eight scans per t_1 increment. Transformation was done using a $\pi/2$-shifted sine-squared bell filter in both dimension and zero-filling to a square matrix of 1024 × 1024 points for a final digital resolution of 2.4 Hz/point. A first-order polynomial baseline correlation was applied in the $f2$ dimension prior to volume integration of the cross-peaks. The average of the equivalent volumes above and below the diagonal was used for analysis. All data processing was done using UXNMR software provided by Bruker. Steady-state 1D NOE experiments on the trisaccharide were done as described before (Michon et al., 1987). The ^{1}H spectrum of a few milligrams of colominic acid was taken at various temperatures up to 343 K, in order to observe the proton coupling constants. As described previously (Michon et al., 1987), proton assignments were obtained from a COSY experiment. Spin simulations were done using LAOCN5 (QCPE) with FTNMR (Hare Research Inc.). The error on the coupling constants was ± 0.3 Hz.

Calculations. The starting geometry of αNeuAc was built from the crystal structure of the β sialic acid methyl glycoside (Flippen, 1973) after proper setting of the anomeric configuration. It was then submitted to a complete refinement of bond lengths, valence, and torsion angles by using the molecular mechanics program MM2(87) (QCPE) (Burket & Allinger, 1982). All calculations were done using the minimized coordinates for the methyl glycoside of αNeuAc (Table I).

For a given disaccharide, the conformational analysis was evaluated using the PFOS approach which included the partitioned contributions arising from van der Waals interactions and torsional and exo-anomeric potential (Tvaroska & Perez, 1986). Rotational barriers of 1.0 and 0.5 kcal/mol were used for ϕ and ψ, respectively. No electrostatic contribution was considered. The ring geometry was treated as invariant, and hydroxylic hydrogen atoms were not taken into account.

Four angles determine the linkage conformation for αNeuAc(2–8)αNeuAc(b–a): ϕ = (bO6–bC2–bO2–aC8), ψ = (bC2–bO2–aC8–aC7), ω_8 = (O7–C7–C8–O8), and ω_7 = (O6–C6–C7–O7). The orientation of the pendant groups for C1 and C9 was defined by ω_1 = (O6–C2–C1–O1A) and ω_9 = (O8–C8–C9–O9). All angles are expressed in degrees. The angles ω_1, ω_7, ω_8, and ω_9 were always set the same for both residues. The ω_7 angle was set at 60°, and separate maps were generated for ω_8 = 60°, −60°, and 180° (g^+,g^-,t). The (ϕ,ψ) maps were calculated in the following way. For a given set of ω_7, ω_8 values, the glycosidic torsional angles ϕ and ψ were stepped in increments of 5° over the angular range which contained low energy minima, −120° to +240° for ϕ and 40° to 220° for ψ. At each point of this grid search, the ω_1 and ω_9 angles were stepped in increments of 20° over the whole angular range, and the minimum energy conformer was selected. Such a procedure allowed severe steric constraints to be relieved between the hydroxymethyl group at C9 and the carboxyl group at C1 across the glycosidic linkage. All the low energy conformers derived from the analysis of such "rigid potential energy surfaces" were refined using the MM2(87) software. From all these minimized conformers, the averages of the ω_7 and ω_8 angles for the three staggered ω_8 conformers were taken and the rigid maps were calculated again using these mean values (Table II). The average glycosidic bridge angle for bC2–bO2–aC8 of 117° was also used.

Helices are customarily described in terms of a set of helical parameters, (n,h), with n being the number of residues per turn of the helix and h being the translation of corresponding residues along the helix axis. The parameter n is derived from the rotation angle (μ) about the helix axis per repeat unit, where $n = 2\pi/\mu$. With set values of glycosidic valence angles and residue geometry, these parameters can be calculated for

Table II: Minimum Energy Conformers for αNeuAc(2–8)αNeuAc

	E^a	ϕ	ψ	ω_7	ω_8	ω_9	ω_1	$\langle O1 \rangle^b$	n	h^c	h/L
G1$^+$	3.2	−45	130	55	70	138	−40	9.1	2.3	4.8	0.8
G2$^+$	0.0	75	100	55	70	138	−20	6.5	3.6	−3.2	−0.5
G3$^+$	2.9	−180	105	55	70	138	−40	6.7	11.3	5.7	0.9
G1$^-$	3.6	−50	120	60	−62	−162	−40	6.3	2.5	2.9	0.7
G2$^-$	0.3	60	115	60	−62	78	−20	7.4	2.2	−4.2	−1.0
G3$^-$	2.3	170	135	60	−62	−162	−40	6.9	2.8	−1.9	−0.5
T1	5.2	15	155	67	179	138	180	3.8	2.9	1.2	0.2
T2	1.0	80	160	67	179	98	180	4.7	3.0	−4.0	0.8

[a] Relative energy in kilocalories per mole. [b] Average distance in angstroms between the four carboxyl oxygen atoms. [c] In angstroms.

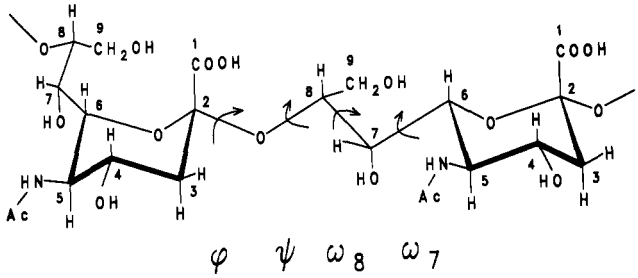

FIGURE 1: Structure of αNeuAc(2–8)αNeuAc showing the four torsion angles which determine the linkage conformation with (O6–C6–C7–O7) = ω_7 = 60° and (O7–C7–C8–O8) = ω_8 = 60°. The orientation of the pendant groups at C1 and C9 is defined by ω_1 = (O6–C2–C1–O1A) and ω_9 = (O8–C8–C9–O9), respectively.

any given value of the set of torsional angles (Sugeta & Miyazama, 1967). The length of the virtual bond (L) between two adjacent linking atoms, namely, O2 and O8, represents the maximum of the possible extension. The quotient h/L yields the percentage of total extension. The chirality is defined by the sign of h, positive for right-handed helices and negative for left-handed helices.

The NOE was calculated using the complete relaxation matrix, under the assumption of isotropic tumbling. The steady-state NOE was calculated as described before (Brisson & Carver, 1983). The 2D NOE was calculated according to Borgias and James (1988). Determination of distances from 2D NOE data was done using the distance extrapolation method (Baleja et al., 1990). The ensemble averaged NOE was calculated as described by Cumming and Carver (1987). For better Boltzman weighting of the NOE, a potential energy map with 1° increments in (ϕ,ψ) was generated from the 5° interval map using cubic spline interpolation. Only $\langle r^{-6} \rangle$ motional averaging was used. Averaging was only done for (ϕ,ψ), the ω_7, ω_8, and ω_9 angles being fixed. For a given ω_7 and ω_8 value, the (ϕ,ψ) potential energy surface for which ω_1 and ω_9 adopted minimum energy conformers was used (see above) and the averaged NOE was calculated separately for ω_9 = 60°, −60°, and 180°. This could be done because no major interglycosidic NOE was observed on the H9 resonances. The relative energy of conformers within a well were modified by first defining a contour level which encompassed a local minima and then changing the energy of the conformers at the grid points within the well by the same amount. The relative population within a well was calculated using the Boltzmann distribution on a 1° × 1° grid interpolated from a 5° × 5° grid.

In order to calculate the NOE, the rotational correlation time of the molecule must be determined. It was estimated from a best fit of the calculated NOE to H3a–H5 and H3e–H5 for various rigid conformers. Correlation times of 8 ns and 0.5 ns were used for simulation of the NOE for colominic acid and the trisaccharide, respectively. The "standard deviation", Sdev, for the NOE was calculated using $N(\text{Sdev})^2 = \sum(\text{NOE}_{exp} - \text{NOE}_{cal})^2$, where N is the number of points.

The $n - h$ plots for poly(A) were generated in a similar manner as described before (Yathindra & Sundaralingam, 1976) using X-ray coordinates (Saenger et al., 1975). Ball and stick models were generated with the SCHAKAL program. Calculations were performed on Micro VAX 3200 and 3500.

RESULTS

In order to understand the conformational behavior of αNeuAc(2–8)αNeuAc (Figure 1), the linkage conformation ϕ, ψ, ω_7, and ω_8, and the orientation of the pendant groups must be determined. The pyranose ring adopts a well-defined

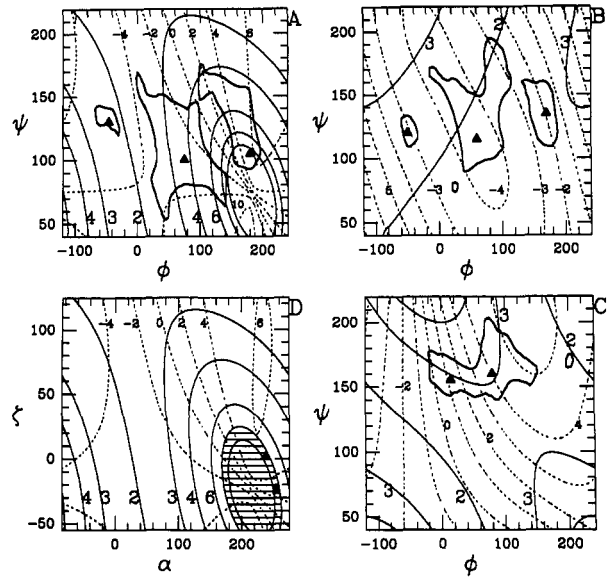

FIGURE 2: Potential energy contour map for αNeuAc(2–8)αNeuAc with (ω_7,ω_8) = (55°,70°) (A), (60°,−62°) (B), and (67°,179°) (C) and ω_1 and ω_9 adopting minimum energy conformers. With respect to the global minimum of each section, the 8, 6, and 10 kcal/mol levels are drawn for (A), (B), and (C), respectively. For (A), from left to right, three seperate wells, WG1$^+$, WG2$^+$, and WG3$^+$, are thus defined. Similarly for (B), three wells WG1$^-$, WG2$^-$, and WG3$^-$ are defined. Local energy minima (Table II) are indicated. The helical parameters n (solid lines) and h (dotted line) are also displayed. For poly(A) (D), the $n - h$ map and the energetically favored helices (dashed area) are shown. The helices with (n,h) = (9,2.8 Å) and (9,5.5 Å) are marked.

$^2C_5$ conformation, and the NAc group at C5 adopts a planar configuration with the H5–C5–N5–HN5 in the trans configuration (Christian & Schultz, 1987).

Potential Energy Calculations. Potential energy calculations were performed in order to assess the (ϕ,ψ) conformational space for the staggered rotamers of ω_8, with ω_7 fixed to the g$^+$ rotamer (Figure 2). The helical parameters, obtained upon propagation of the molecule, are also plotted. Three (ϕ,ψ) maps were represented where the ω_1 and ω_9 rotamers were allowed to adopt minimum energy conformers for each setting of the linkage conformation. The ω_7 and ω_8 angles were optimized by molecular mechanics calculations. For the (ω_7,ω_8) = (55°,70°) map (Figure 2A), three major wells, WG1$^+$, WG2$^+$, and WG3$^+$, which encompass minima G1$^+$, G2$^+$, and G3$^+$ (Table II) are defined by the 8 kcal/mol level with respect to the global minimum. For the (ω_7,ω_8) = (60°,−62°) map (Figure 2B), three separate wells, WG1$^-$, WG2$^-$, and WG3$^-$, could be defined by the 6 kcal/mol level above the G2$^-$ conformer (Table II). The (ϕ,ψ) energy map for (ω_7,ω_8) = (67°,179°) maps was more restricted, and only the 10 kcal/mol level with respect to minimum T2 (Table II) is shown in Figure 2C. Although other local minima could be found within these wells, only the areas defined by these wells were useful in interpreting the NOE results. Relevant parameters for various low-energy conformers are given in Table II. Molecular mechanics calculations were performed for various conformers within these wells (data not shown). It was found that these conformers were stable, the linkage angles not changing significantly upon complete minimization. Multiple orientations of ω_9 were also favorable. The ω_1 orientation was mostly restricted to conformers around −170° and −40°.

In order to estimate the role of the charge, the average distance between the four oxygen atoms for the carboxyl group is given in Table II. The ω_8 trans rotamer is expected to be

Table III: Experimental 2D NOE Volumes[a] with 75 ms of Mixing Time for Colominic Acid and Calculated Relative NOE[b]

		average[c]			minima		
protons	exp	⟨G⁺⟩	⟨G⁻⟩	⟨T⟩	G1⁺	G2⁺	G3⁺
H3a–H3e	100	100	100	100	100	100	100
H3a–H8	9	8–11	8	2	32–41	2	28
H3e–H8	5	5–6	5	2	17–23	2	47
H3a–H7	3	3	2	2	4–6	2	74
H3e–H7	3	3	1	1	3	3	60
H5–H8	4	2–4	3	2	12–16	2	5
H3a–H5	24	22	22	22	24	22	30
H3e–H5	12	12	11	11	12–14	11	16
Sdev[d]		1–2	2–3	4	10–15	4	34
H8–H6	28	26–33	5–6	7	30–42	26–30	40
H8–H7	30	20–24	27	9	22–31	19–22	31
H3a–H9[e]	2	2–19	1–6	1	7–80	1	3
H3e–H9[e]	1	1–11	1–3	1	4–57	1	4
H7–H9[e]	11	3–4	6–18	4–19	5	3	4

[a] Estimated error = ±25%. [b] The H3a–H3e NOE is set to 100. (ω_7,ω_8) for G⁺ conformers = (55°,70°), for ⟨G⁻⟩ = (60°,−62°), and for ⟨T⟩ = (67°,179°). (ϕ,ψ) for G1⁺ = (−45°,130°), for G2⁺ = (75°,100°), for G3⁺ = (180°,105°). Significant changes for ω_9 = 60°, −60°, and 180° are shown. [c] (ϕ,ψ) ensemble averaged NOE. Relative energies (in kilocalories per mole) for wells WG1⁺, WG2⁺, and WG3⁺ are 1.2:0:3 and for wells WG1⁻, WG2⁻, and WG3⁻ are 0.5:0:2. [d] Standard deviation of the fit for six mixing times and for the first 8 volumes only. The calculated NOE range for H9R and H9S is also included.

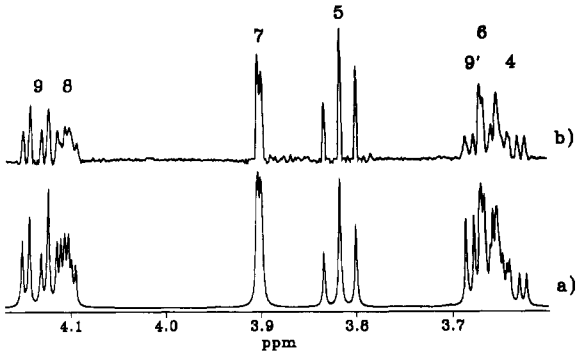

FIGURE 3: Partial ^{1}H NMR spectra of colominic acid at 600 MHz and 343 K: (a) spin simulated spectrum and (b) resolution enhanced spectrum.

less favored in solution due to the close proximity of the charged groups between adjacent residues, while for all the gauche conformers the carboxyl groups are further apart.

Colominic Acid. Colominic acid, which has a proton spectrum identical to that of the group B meningococcal polysaccharide (data not shown), was used since it was more readily available. The choice of counterion, the pH, and the molecular weight fraction of the polymer are important factors which were considered in order to get a sample as homogeneous as possible and a stable sample which did not degrade with time. The high molecular fraction of commercially available colominic acid (Na^+ salt) was selected by gel filtration. The pH was adjusted to 7. Different samples were prepared which always gave the same spectra (Michon et al., 1987). Especially, the H8 and H9 resonances were resolved which permitted the detection of NMR parameters which were crucial in assessing the solution conformation of colominic acid. In order to determine more accurately the vicinal proton coupling constants for colominic acid, the ^{1}H spectrum was obtained at 343 K (Figure 3). All multiplets could be resolved and correctly spin simulated to obtain accurate parameters. The proton coupling constants did not change with temperature (Lindon et al., 1984). Proton coupling constants were found to be the same as those for residue *b* of the trisaccharide at 300 K (Michon et al., 1987), except for *J*(H8,H9′) which was 5.5 Hz instead of 6.9 Hz.

The 2D NOE experiment with a mixing time of 75 ms, at 600 MHz, and 288 K, for colominic acid is shown in Figure 4. The volumes that could be accurately measured are given

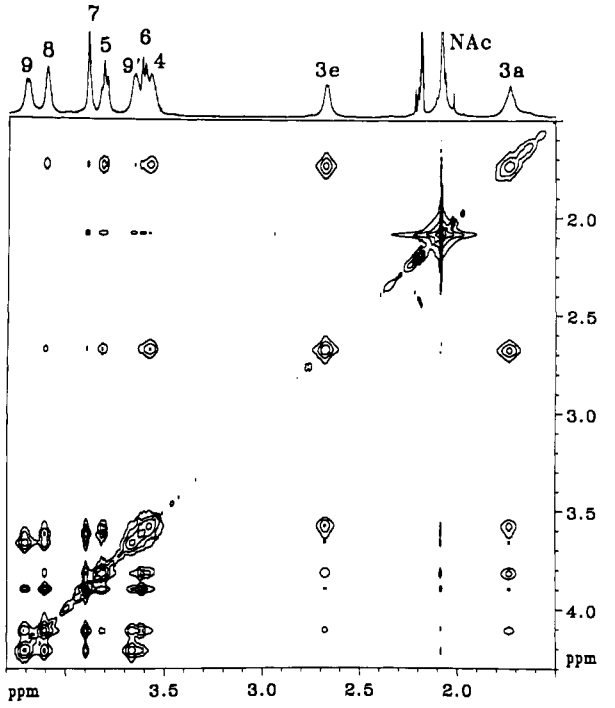

FIGURE 4: 2D NOE spectrum at 600 MHz and 288 K of colominic acid. The mixing time was 75 ms. The 1D spectrum is shown on top along the *f*2 axis.

in Table III, and some are plotted in Figure 5. All NOE calculations were done using the coordinates for the disaccharide (*b*–*a*). A dimer can be used to simulate the NOE's because the most favorable conformers form extended helices when propagated (Figure 2) with pitches (*nh*) greater than 5 Å. Hence, long-range interactions between nonadjacent residues will not be important. For colominic acid, the NOE between two protons was taken as the sum of the inter- and intraresidue NOE of the equivalent pair. For example, the H3a–H7 NOE was the sum of the *b*H3a–*b*H7 NOE and the *b*H3a–*a*H7 NOE. For some conformers, the inter- and intraresidue contributions were comparable.

The NOE's for H3a–H5 and H3e–H5 are dominated by the intraresidue NOE only. From the 2D NOE buildup rates, using the distance extrapolation approximation (Table IV), the H3a–H5 and H3e–H5 distances were found to be 2.5 and 3.3 ± 0.2 Å, respectively. Although the H3a–H5 distance is

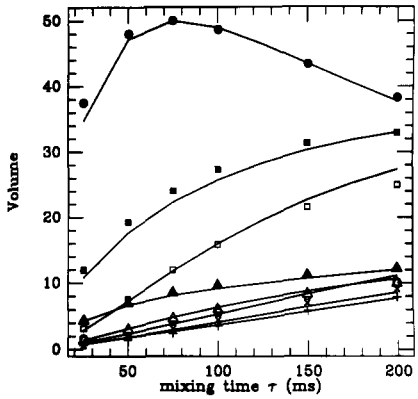

FIGURE 5: 2D NOE buildup rate for colominic acid. The experimental volumes for (H3a–H3e)/2 (●), H3a–H5 (■), H3e–H5 (□), H3a–H8 (▲), H3e–H8 (△), H5–H8 (○), H3a–H7 (×), and H3e–H7 (+) are shown. The (ϕ,ψ) ensemble averaged theoretical NOE buildup rates (solid lines) using the potential energy map for $\omega_7 = 55°$, $\omega_8 = 70°$ (Figure 2A) with an altered relative energy for wells WG1$^+$, WG2$^+$, and WG3$^+$ of 1.2:0:3 kcal/mol and the ω_9 value which gave the best fit are also plotted.

Table IV: Distances for αNeuAc Obtained from Minimized Coordinates, from Distance Extrapolation[a] of Calculated 2D NOE Using Conformer G1$^+$, and from the Experimental 2D NOE[b] buildup Rate for Colominic Acid

protons	coordinates	NOE calcd	NOE exptl
H3a–H3e	1.79		
H3a–H5	2.51	2.5	2.5
H3e–H5	3.74	3.3	3.3

[a] a_0 from fit of $y = a_0 + a_1x + a_2x^2$, where $(y/r_0)^6 = V/V_0$, V_0 = H3a–H3e volume, r_0 = 1.79 Å, V = cross-peak volume, and x = mixing times of 25, 50, 75, 100, 150, and 200 ms. [b] Estimated error = 0.2 Å.

in agreement with the distance of 2.51 Å calculated from the coordinates of Table I, a distance of 3.74 Å is expected for H3e–H5. However, if the buildup rates are calculated using the coordinates of conformer G1$^+$ and the H3e–H5 distance extrapolated from the calculated volumes, a value of 3.3 Å is obtained. The reason for this discrepancy is that higher order effects are neglected in the distance extrapolation method (Landy & Rao, 1989). Hence, in order to account for correct summation of the inter- and intraresidue NOE's and the complete spin geometry, a full matrix analysis was always used.

The NOE also depends on all pairs on interproton distances and thus on ϕ, ψ, ω_7, ω_8, and ω_9. For motional averaging, the NOE must be averaged in a certain way depending on the rates of internal motion (Kessler et al., 1988). In this case only $\langle r^{-6} \rangle$ averaging was considered, since the mode of averaging will not affect any of the conclusions reached in this study. The r^{-6} terms for a conformer were weighted according to the Boltzmann distribution function.

The NOE's were analyzed using a model where the molecule was allowed to sample energetically favored conformers over (ϕ,ψ) with the ω_8 and ω_9 rotamers adopting staggered conformers only. The ω_7 angle was kept fixed to the g$^+$ rotamer. Since, in general, NOE's that were highly dependent of ϕ and ψ were not greatly affected by the value of ω_9, the potential energy map where ω_9 is allowed to freely rotate could be used to calculate the (ϕ,ψ) ensemble averaged NOE for different values of ω_9. The NOE's for H3a–H8, H3e–H8, H3a–H7, H3e–H7, and H5–H8 satisfied this condition and thus could be used to assess the (ϕ,ψ) linkage conformation. The NOE's between H3a–H9 and H3e–H9 were not used because they were highly dependent on ω_9, and the H9 assignment to either

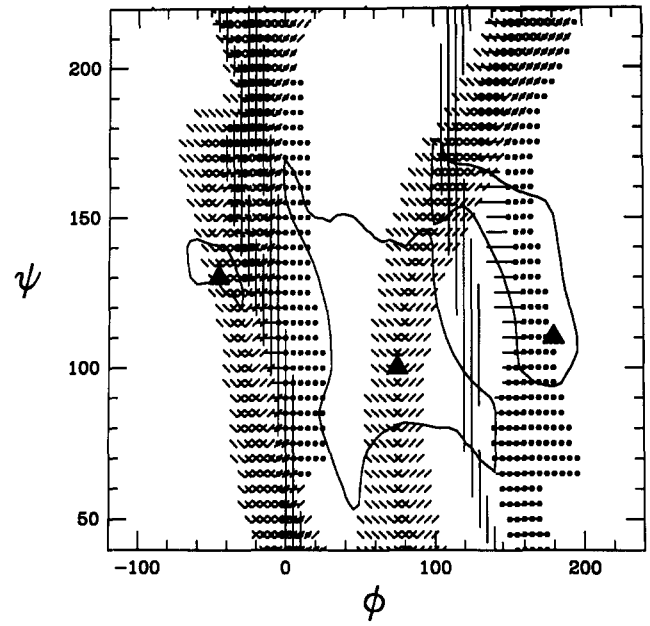

FIGURE 6: NOE constraints map of colominic acid for a mixing time of 75 ms. The calculated relative NOE's using the full relaxation matrix, which satisfy the experimental NOE's (Table III) with an error bound of ±25% are plotted as a function of (ϕ,ψ), with $\omega_7 = 55°$, $\omega_8 = 70°$. The NOE constraints for H3a–H8 (–), H3e–H8 (|), H3a–H7 (/), H3e–H7 (\), and H5–H8 (○) relative to H3a–H3e are displayed. The maps for $\omega_9 = 60°$, –60°, and 180° are overlaid. The 8 kcal/mol levels which define the three major energy wells WG1$^+$, WG2$^+$, and WG3$^+$ (left to right) around the G1$^+$, G2$^+$, and G3$^+$ confomers (Table II) are also shown.

H9R or H9S was ambiguous. Still, these calculated NOE's for different values of ω_9 were within the range of the experimental ones. Conversely, the NOE's for H8–H6, H8–H7, and H7–H9 could be used to determine the orientation of the exocyclic chain since they were not highly dependent on (ϕ,ψ).

The conformation of the exocyclic chain was determined from the proton vicinal coupling constants which are dependent on the torsional angle H–C–C–H and from NOE's. From a spin simulation of the ^{1}H spectrum at 343 K, J(H6,H7) and J(H7,H8) were found to be 1.0 and 2.3 Hz, respectively (Figure 3). Also, the strong NOE for H8–H6 and H5–H7 (Figure 4), indicated that the $\omega_7 = 60°$ and $\omega_8 = 60°$ rotamers were predominant in solution. For the hydroxymethyl group at C9, J(H8,H9) and J(H8,H9′) were 4.5 and 5.5 Hz, indicating that the staggered rotamers for ω_9 were all accessible. These results are similar to the ones obtained for the corresponding linkage in the trisaccharide (Michon et al., 1987). However, an NOE between the H7 and the H9 resonance indicated that the other rotamers for ω_8 were also present. Most probably, the g$^-$ rotamer was present due to the small J(H8,H7) = 2.3 Hz and the large H8–H7 NOE, which can arise from both gauche rotamers (Table III).

Five NOE's could be used to evaluate the (ϕ,ψ) linkage conformation, namely those for H3a–H8, H3e–H8, H3a–H7, H3e–H7, and H5–H8. An NOE constraints map was calculated to determine if all sets of NOE's can satisfy a unique conformer. The NOE was calculated for each grid point and if its value falls within error bounds of the experimental NOE, it was indicated on the map. For g$^+$ rotamers of ω_7 and ω_8, three maps were calculated for staggered rotamers of ω_9 and overlaid. No unique energetically favorable conformer satisfied the five experimental NOE constraints (Figure 6). Similar results were obtained for the other staggered rotamer of ω_8.

The experimental NOE's were successfully simulated using motional averaging over (ϕ,ψ) (Table III, Figure 5). For the

Table V: Experimental 1D NOE[a] for αNeuAc(2–8)αNeuAc(2–8)βNeuAc (*c–b–a*) and Calculated Relative NOE[b]

		average[c]			minima		
protons sat. obsd	exptl	⟨G⁺⟩	⟨G⟩	⟨T⟩	G1⁺	G2⁺	G3⁺
*c*H3a–*c*H3e	100	100	100	100	100	100	100
*c*H3a–*b*H8	16	10–17	14	3	39–44	1	19–21
*c*H3a–*b*H6	3	2	1	4	6	1	12
*c*H3a–*c*H4	31	28	27	28	28	27	33
*c*H3a–*c*H5	53	55	57	59	51–54	56	78
*c*H3a–*b*H7	–[d]	3	2	2	5	2	80
*c*H3a–*c*H6	6	6	4–7	8	6	6	8
*c*H3a–*c*H7	3	4	3	3	4	4	6
*c*H3e–*c*H3a	100	100	100	100	100	100	100
*c*H3e–*b*H8	7	4–7	8	5	13–16	1	58–65
*c*H3e–*b*H6	4	1	1	6	2	1	22
*c*H3e–*c*H4	46	55–64	54	52	63–102	51	66
*c*H3e–*c*H5	21	22	21	22	20–26	21	23
*c*H3e–*b*H7	–[d]	4	1	2	3	5	55
*c*H3e–*c*H6	7	6–8	4–8	8	7–12	6	8
*c*H3e–*c*H7	–[e]	2	2	2	4	2	3
Sdev[f]		4–6	4	5	9–19	6	40
*b*H8–*b*H7	100	100	100	100	100	100	100
*b*H8–*b*H6	114	102–106	12–23	71–87	108–122	104	240
*b*H8–*b*H3a	21	16–19	12–14	6	33–64	2	43
*b*H8–*b*H3e	14	7	6–8	8	12–21	2	130
*b*H8–*b*H5	–[e]	12	8	5	37–48	3	13

[a] Estimated error = ±25%. [b] The reference NOE is set to 100. (ω_7,ω_8) for G⁺ conformers = (55°,70°), for ⟨G⟩ = (60°,–62°), and for ⟨T⟩ = (67°,179°). (ϕ,ψ) for G1⁺ = (–45°,130°), for G2⁺ = (75°,100°), and for G3⁺ = (180°,105°). Significant changes for ω_9 = 60°, –60°, and 180° are shown. [c] (ϕ,ψ) ensemble averaged NOE. Relative energies (in kilocalories per mole) for wells WG1⁺, WG2⁺, and WG3⁺ are 0.4:0:3 and for wells WG1⁻, WG2⁻, are 0.5:0:2. [d] Resonances *c*H5 and *b*H7 overlap. [e] Absolute NOE <1 ± 1. [f] For *c*H3a and *c*H3e NOE's only.

ω_7 = 55°, ω_8 = 70° energy surface, three major wells, WG1⁺, WG2⁺, and WG3⁺, which encompass conformers G1⁺, G2⁺, and G3⁺ can be defined by the 8 kcal/mol level with respect to the global minimum G2⁺ (Figure 2A). With the relative energy for minima G1⁺, G2⁺, and G3⁺ of 3:0:3 kcal/mol obtained from the potential energy calculations, the relative population of well WG1⁺ was 99%, while the other wells had less than 1% occupancy. The (ϕ,ψ) ensemble averaged NOE's calculated using this distribution were the same as those calculated using the single minimum conformer G2⁺, since for all conformers within well WG2⁺, interglycosidic NOE's were small, compared to those for conformer G1⁺ or G3⁺ (Table III). Hence, poor agreement was obtained with the experimental values. However, it was observed that the NOE's showed very little dependence on ψ and that interglycosidic NOE's had maxima near conformers G1⁺ and G3⁺. For conformer G1⁺, H3a interglycosidic NOE's are bigger than those of H3e, while for conformer G3⁺ the reserve is true. Hence, a slight increase in the population of well WG1⁺, would lead to good agreement between the averaged NOE's and the experimental data. The occupancy of well WG3⁺ must remain low, or the relative magnitude of the H3a–H3e NOE's would change. A relative energy between wells WG1⁺, WG2⁺, and WG3⁺ of 1.2:0:3 kcal/mol, equivalent to a population of 13:86:1, was found to give the best fit. Only the ratio for WG1⁺ and WG2⁺ was altered, the one for WG2⁺ and WG3⁺ being kept fixed as that found from the potential energy calculations. The (ϕ,ψ) ensemble averaged NOE's were calculated for the three staggered ω_9 rotamers and exhibited no major dependency on ω_9, except those involving H9 (Table III).

Since other rotamers for ω_8 can be present, (ϕ,ψ) ensemble averaged NOE calculations were also done for all staggered ω_8 rotamers. For the g⁻ rotamer, energy wells similar to those for the g⁺ rotamer were observed, and a good fit of all NOE's, except for H8–H6, could be obtained (Table III). Distinct wells WG1⁻, WG2⁻, and WG3⁻ could be defined by the 6 kcal/mol level with respect to conformer G2⁻ (Figure 2B). The relative energy of well WG1⁻ had to be modified for a good fit. The relative energy of well WG3⁻ was not altered. Relative energies for wells WG1⁻, WG2⁻, and WG3⁻ of 0.5:0:2 kcal/mol equivalent to a population of 8:90:2 gave the best agreement between the averaged NOE's and the experimental data. Poor agreement was found for the trans rotamer (Figure 2C), since no energetically favored conformers near ϕ = –50° were present where strong interglycosidic NOE's with the two H3 geminal resonances occurred.

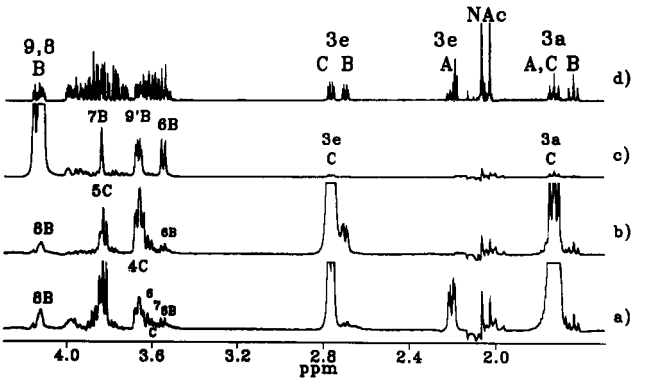

FIGURE 7: 1D NOE difference spectra of αNeuAc(2–8)αNeuAc(2–8)βNeuAc (*c–b–a*) for saturation of H3a of residue *a* and *c* (a), of H3e of residue *c*, and of H8 and H9 of residue *b* (c) are shown along with the 1D spectrum (d).

Trisaccharide. NMR experiments were performed on the trisaccharide in order to compare the linkage conformation of the polymer to the one of the linkage *c–b* of the trisaccharide αNeuAc(2–8)αNeuAc(2–8)βNeuAc, (*c–b–a*). The 1D NOE spectra for the trisaccharide at 600 MHz and 288 K are plotted in Figure 7, and the NOE data are given in Table V. By performing the experiments at a lower temperature, the correlation time of the molecule was decreased, leading to bigger negative NOE's, which could be more accurately integrated. The chemical shift assignments and coupling constants were similar to those reported before (Michon et al., 1987).

As for colominic acid, a strong NOE between *b*H8 and *b*H6, J(*b*H8,*b*H7) = 2.3 Hz, and J(*b*H7,*b*H6) = 1 Hz indicated that

the $\omega_7 = 60°$ and $\omega_8 = 60°$ rotamers were predominant in solution. Due to partial overlap of *b*H9 and *b*H8 resonances, the *b*H9 resonance could not be selectively saturated and the small NOE between H9 and H7, which might indicate the presence of other ω_8 rotamers, could not be evaluated, as observed for colominic acid.

Four sets of NOE's could be used to evaluate the (ϕ,ψ) linkage conformation distribution, namely interglycosidic NOE's between *c*H3a–*b*H8, *c*H3e–*b*H8, *c*H3a–*b*H6, and *c*H3e–*b*H6. Although the *c*H3a–*b*H7 and *c*H3e–*b*H7 NOE's could be observed, the overlap of the *b*H7 resonance with the *b*H5 resonance prevented their quantification. The *b*H8–*c*H5 NOE was detected, but its magnitude (<1) and the noisy baseline prevented its accurate determination.

All NOE calculations were done using the coordinates of the disaccharide αNeuAc(2–8)αNeuAc, which correspond to residues *c*–*b* of the trisaccharide (Table V). The NOE constraints maps were similar to the ones for colominic acid, and they did not show the presence of a preferred conformer in solution (data not shown). However, the (ϕ,ψ) ensemble averaged NOE's, using modified energy surfaces for the gauche rotamers of ω_8, were able to reproduce adequately the experimental NOE's. Relative energies for $WG1^+$, $WG2^+$, and $WG3^+$ of 0.4:0:3 kcal/mol, equivalent to a population of 20:79:1, were found to increase the magnitude of the interglycosidic NOE's comparable to those of the observed ones. The (ϕ,ψ) ensemble averaged NOE calculations for g^- and the trans rotamers of ω_8 were performed using the same potential energy surfaces as for colominic acid.

Discussion

The conformation of colominic acid has been previously discussed by a number of authors, and all have relied on interpretation of NMR results. Lindon et al. (1984) determined, from NMR at 360 MHz, that H7 and H8 were gauche and molecular mechanics calculations were used to assess the rotational barriers about the C7–C8 bond. All staggered rotamers were found to be accessible with barriers of about 10 kcal/mol. The ^{13}C NMR spin-lattice relaxation times, were interpreted as suggesting that the α(2–8)NeuAc polysaccharide tumbled isotropically in solution as a rigid species. Michon et al. (1987) studied differences in NOE's at 500 MHz between the polysaccharide and trisaccharide and from a qualitative interpretation of the NOE's only, it was proposed that the polysaccharide adopted a different conformation from the trisaccharide. Recently, Yamasaki and Bacon (1991), from a quantitative analysis of 2D NOE's at 500 MHz using rigid conformers, suggested that the polysaccharide adopts ordered helical structures in solution.

In our study, both the results and their interpretation differ from those of Yamasaki and Bacon (1991). Different chemical shifts for the polymer were observed, which could possibly be attributed to sample preparation. While the H8 and the downfield H9 resonance overlapped for their sample, they were resolved in this study. Thus, the overlap of the H8 and H9 resonances prevented these authors from determining the C8 stereochemistry. Using rigid models and steric constraints, they proposed ordered helical structures for the following (ϕ,ψ) ranges: (−60° to 0°, 115° to 175°) for $\omega_8 = 60°$ and (90° to 120°, 55° to 175°) for $\omega_8 = -60°$. Their (ϕ,ψ) ranges correspond to the two areas in the NOE map (Figure 6), where some NOE constraints intersect the most. From models, they estimated the number of turns per helix, n, to be from 3 to 4 and the pitch (nh) to be from 9 to 11 Å. Their helical parameters were overestimated by a factor of 2, since it is difficult from molecular models alone to determine the rotation angle (μ) along the helix axis between two residues, from which $n = 2\pi/\mu$. Values of n greater than 2 for $\omega_8 = 60°$ and also n greater than 2 for $\omega_8 = -60°$ correspond to their (ϕ,ψ) ranges (Figure 2).

In this study, NOE data at 600 MHz for the polysaccharide and the trisaccharide were interpreted by invoking flexibility about the exocyclic linkages. The best fit of the NOE data for colominic acid (Table III, Figure 5) was obtained from a (ϕ,ψ) ensemble average over the whole energy surface. Proton coupling constants and NOE data indicated that the g^+ rotamers for ω_7 and ω_8 were predominant in solution. However, flexibility had to be invoked about the C7–C8 bond due to NOE's which could only arise from other rotamers, most probably the g^- one. From the determination of the proton coupling constants for the H9 resonances, all staggered conformers for the hydroxymethyl group at C9 were postulated to be accessible. Hence, due to the wide range of conformations which can be sampled, the polysaccharide is suggested to exist predominantly as a random coil in solution.

As Perez and Vergelati (1985) noted in their study of polysaccharide helical structures, the spatial organization of the polymer chain can be defined by consecutive fragments which have well-defined helical parameters. These local helices can also be referred to a pseudohelices. Compared to other homopolysaccharides, α(2–8)-linked sialic acid ranks first in terms of displaying a wide range of helical structures (Figure 2). Obviously, the presence of four bonds in the linkage junction amplifies the number of allowed conformational states, as well as the number of helical types which can be generated. The helical parameters for a few low-energy conformers are given in Table II. Three helices for the g^+ rotamers of ω_7 and ω_8 are shown in Figure 8. Whenever the values $h = 0$ or $n = 2$ are crossed, the chirality of the helix changes. The $n = 2$ helix corresponds to a zigzag planar configuration, while $h = 0$ corresponds to cyclic oligomers. Conformers with small values of h would fold back on themselves after n residues. For the $\omega_8 = g^+$ rotamer, most energetically favored conformers could form local helices, since the $h = 0$ line crosses a region where values of n were greater than 4 (Figure 2A). Also, high-order helices can form with $n > 6$, while for the other ω_8 rotamers n is from 2 to 3 only. For the g^+ rotamer of ω_8 in the high-order helical region, a small change in linkage conformation leads to a large change in helical parameters. Hence, the topological features of the polymer can change with little change in energy. Such properties would be favorable to topological rearrangements from disordered random coils to more ordered conformations which promote the formation of the helical epitope.

For a polysaccharide, the NOE's will be averaged over all the conformers sampled in solution. If a predominant conformer or a pseudohelix exists in high enough proportion, this should be reflected in the NOE's, and a NOE constraints map could detect the presence of a preferred conformer. If more than one conformer satisfied the constraints, or no preferred conformer was found, then the presence of molecular flexibility must be invoked to explain the observed NOE's. Even if the NOE's indicate the presence of a preferred conformer and the motional averaging calculations still satisfy the experimental conditions, motional flexibility cannot be ruled out.

For the case of colominic acid and the trisaccharide, the NOE's are best explained by motional averaging. A small proportion of conformers was found to greatly influence the averaged NOE's, since their NOE's were of much greater magnitude than the majority of conformers, as can be seen by comparing the H3a–H8 and H3e–H8 NOE's for con-

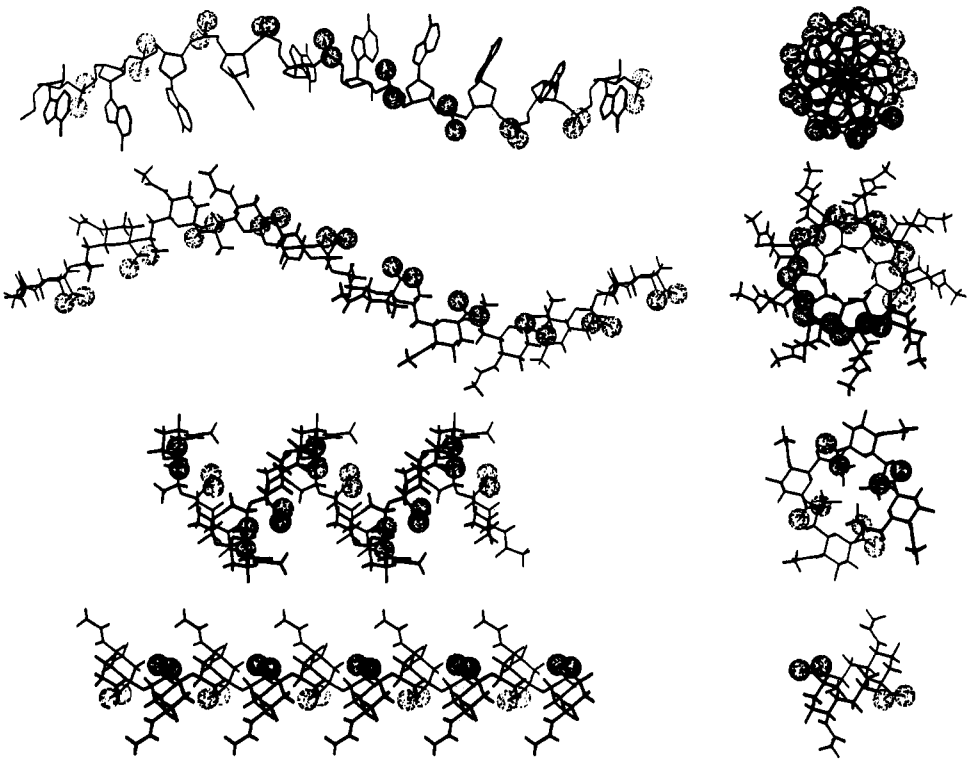

FIGURE 8: Side and top view with respect to the helix axis for helices of $\alpha(2-8)NeuAc_{10}$ which arise from propagation of conformers $G1^+$, $G2^+$, and $G3^+$. The linkage conformation have been slightly altered to give integral helices of $n = 2$, 4, and 9. The $n = 9$, $h = 5.5$ Å, helix for poly(A) is shown on top. The charged groups in the molecules are represented as spheres.

formers $G1^+$ and $G2^+$ (Tables III and V). The relative energy of the potential energy wells had to be altered in order to reproduce the observed NOE's. Empirical potentials, which neglect molecular flexibility, electronic interactions, and solvent effect, are used only to crudely estimate the allowable conformational space. The rigid potential would also overestimate barriers to interconversion. The NOE data can thus be used to test different population distributions calculated from empirical potential energy functions (Cumming & Carver, 1987).

For colominic acid a relative population between wells $WG1^+$ and $WG2^+$ of 15:100 was found to reproduce the NOE's correctly. For the trisaccharide, a ratio of 25:100 for the same wells was needed. The relative population of well $WG3^+$ to well $WG2^+$ must remain low (1–2%) in both cases or the He3–H8 would become larger than the H3a–H8 NOE. Hence, difference in linkage conformation between the polymer and short oligosaccharides can be explained as arising from slight changes in the relative population distribution of conformers in solution, as opposed to different rigid conformations (Michon et al., 1987).

The above model for the conformational behavior of colominic acid in solution has important biological implications. The cross-reactivity of IgM^{NOV} with both the $\alpha(2-8)$NeuAc polymer and poly(A) can now be rationalized (Kabat et al., 1988), since they both can adopt similar helices (Figure 2). From the crystal structure of trinucleoside diphosphate of adenosine, a model for the poly(A) helix was proposed with $n = 9$ and $h = 2.82$ Å (Saenger et al., 1975). Energetically preferred conformers due to favorable base stacking can form helices from $n = 8$ to 12 (Yathindra & Sundaralingam, 1976). Therefore, helices for the $\alpha(2-8)$NeuAc polymer and poly(A) can easily be generated which have similar helical parameters. The $n = 9$ helix for both polymers is show in Figure 8. There is not only a similarity in the spatial distribution of charges between the carboxyl groups of $\alpha(2-8)$-linked sialic acid and the phosphate group of poly(A) but also a striking resemblance between the helical parameters of both polymers (Figure 2). This observation would tend to suggest that the conformational epitope occurs within one turn of the helix of $\alpha(2-8)$-linked sialic acid or poly(A). Since the energetically preferred helices of poly(A) have more than 8 residues per helical turn, it is proposed that the conformational epitope for the $\alpha(2-8)$NeuAc polymer probably occurs within a high-order helix which has an extended conformation (Figure 8). However, there is so far no indication of the exact number of residues within this helix that actually bind to group B polysaccharide specific antibodies.

The unusual length requirement of $\alpha(2-8)$-linked sialic acid oligosaccharides to bind to group B meningococcal polysaccharide specific antibodies can also be rationalized. Jennings et al. (1985) and Finne and Makela (1985) observed that at least a decasaccharide was needed to inhibit or bind to these antibodies. Also, for large oligomers of up to 17 sialic acid residues, the inhibitory properties did not maximize but steadily progressed with increasing size. Hayrinen et al. (1989) showed that the critical chain length for binding was 10 units which contributed 90% of the binding energy. The binding for longer oligomers also steadily progressed with increasing size but with minor contributions to the binding energy from the additional residues. Because of the limitations of the size of an antibody site (maximum 6 or 7 residues) (Kabat, 1960), these observations do not imply that the antibody was binding to as many as 10 or more consecutive residues, rather that at least 10 residues are required for the recognition site to form. If the conformational epitope corresponds to a high-order helix with an extended helical conformation, as suggested from cross-reactivity of IgM^{NOV} to poly(A), large oligosaccharides would be required in order for the epitope to form. Since polysaccharides have to undergo topological rearrangements from disordered random coils to more ordered conformations favorable to the formation of the helical epitope and because of the intrinsic versatility of $\alpha(2-8)$-linked sialic acid, it is

unlikely that the epitope would occur in any short oligosaccharide sequence. In addition for the decasaccharide, the conformational behaviors of the reducing and nonreducing residues are expected to be different from that of the inner residues, as observed for the trisaccharide and colominic acid (Michon et al., 1987). The continued increase in binding above 10 units could be attributed to the length stabilization of the epitope, i.e., the increased probability of the presence of the epitope.

The poor immunogenicity of the group B polysaccharide probably arises from the recognition of a helical structure which is also an integral component of the neural cell adhesion molecule N-CAM (Finne et al., 1983). Despite structural mimicry with mammalian tissue, antibodies specific for the α(2–8)-linked sialic acid homopolymer can be produced and from the examples where binding studies have been reported (Jennings et al., 1985; Finne & Makela, 1985; Hayrinen et al., 1989; Kabat et al., 1988) all are specific for the extended helical epitope. Because our conformational studies indicate that this epitope is only a minor contributor to the total number of epitopes available, we must therefore presume that the dominance of this epitope in the immune response must be the result of immunological selection. The failure of the immune system to produce antibodies specific for the more populous lower order helices present in the polysaccharide random coil probably occurs because these short helices are conformationally similar to the ones found in shorter sialyl oligomers. These short α(2–8)NeuAc oligosaccharides are also present in human tissue (Finne et al., 1983), and the production of specific antibody to them appears to be even more stringently avoided.

ACKNOWLEDGMENTS

We thank Francis Michon for critical review of the manuscript and Robert Pon for help in sample preparations. We are grateful to Andy Byrd and Bill Eagan for access to a preliminary manuscript on NOE analysis.

REFERENCES

Baleja, J. D., Moult, J., & Sykes, B. D. (1990) *J. Magn. Reson 87*, 375–384.

Bodenhausen, G., Kogler, H., & Ernst, R. R. (1984) *J. Magn. Reson. 58*, 370–388.

Borgias, B. A., & James, T. L. (1988) *J. Magn. Reson. 79*, 493–512.

Brisson, J. R., & Carver, J. P. (1983) *Biochemistry 22*, 1362–1368.

Burket, U., & Allinger, N. L. (1982) *Molecular Mechanics*, ACS Monograph Series 177, American Chemical Society, Washington, DC.

Christian, R., & Schulz, G. (1987) *Carbohydr. Res. 162*, 1–11.

Cumming, D. A., & Carver, J. P. (1987) *Biochemistry 26*, 6664–6676.

Finne, J., & Makela, P. H. (1985) *J. Biol. Chem. 260*, 1265–1270.

Finne, J., Finne, V., Deagostini-Bazin, H., & Goridis, C. (1983) *Biochem. Biophys. Res. Commun. 112*, 482–487.

Flippen, J. L. (1973) *Acta Crystallogr. B29*, 1881–1886.

Hayrinen, J., Bitter-Suerman, D., & Finne, J. (1989) *Mol. Immunol. 26*, 523–529.

Jennings, H. J. (1989) *Microbiol. Immunol. 10*, 151–165.

Jennings, H. J. (1990) *Curr. Top. Microbiol. Immunol. 150*, 97–127.

Jennings, H. J., Katzenellenbogen, E., Lugowski, C., Michon, F., Roy, R., & Kasper, D. L. (1984) *Pure Appl. Chem. 56*, 893–905.

Jennings, H. J., Roy, R., & Michon, F. (1985) *J. Immunol. 134*, 2651–2657.

Kabat, E. A. (1960) *J. Immunol. 84*, 82–85.

Kabat, E. A., Liao, J., Osserman, E. F., Gamian, A., Michon, F., & Jennings, H. J. (1988) *J. Exp. Med. 168*, 699–711.

Kessler, H., Griesinger, C., Lautz, J., Muller, A., van Gunsteren, W. F., & Berendsen, H. J. C. (1988) *J. Am. Chem. Soc. 110*, 3393–3396.

Landy, S. B., & Rao, B. D. N. (1989) *J. Magn. Reson. 83*, 29–43.

Lindon, J. C., Vinter, J. G., Lifely, M. R., & Moreno, C. (1984) *Carbohydr. Res. 133*, 59–74.

Michon, F., Brisson, J. R., & Jennings, H. J. (1987) *Biochem. 26*, 8399–8405.

Perez, S., & Vergelati, C. (1985) *Biopolymers 24*, 1809–1822.

Saenger, W., Riecke, J., & Suck, D. (1975) *J. Mol. Biol. 93*, 529–534.

Sugeta, H., & Miyazawa, T. (1967) *Biopolymers 5*, 763–679.

Tvaroska, I., & Perez, S. (1986) *Carbohydr. Res. 149*, 389–410.

Yamasaki, R., & Bacon, B. (1991) *Biochem. 30*, 851–857.

Yathindra, N., & Sundaralingam, M. (1976) *Nucleic Acids Res. 3*, 729–747.